International Conference on Computational Methods in Marine Engineering
MARINE 2011
L.Eça, E. Oñate, J. García, T. Kvamsdal and P. Bergan (Eds)

CFD IN SHIP HYDRODYNAMICS – RESULTS OF THE GOTHENBURG 2010 WORKSHOP

LARS LARSSON[*], FREDERICK STERN[†] AND MICHEL VISONNEAU[+]

[*] Chalmers University of Technology
Department of Shipping and Marine Technology
SE-41296 Gothenburg, Sweden
Email: lars.larsson@chalmers.se, web page: http://www.chalmers.se/smt/EN

[†] IIHR—Hydroscience & Engineering
The University of Iowa
100 C. Maxwell Stanley Hydraulics Laboratory
Iowa City, Iowa 52242-1585, USA
Email: frederick-stern@uiowa.edu, web page: http://www.iihr.uiowa.edu

[+] ECN/CNRS
Fluid Mechanics Laboratory - UMR6598
Centrale Nantes BP 92101
44321 Nantes Cedex 3 – France
Email: michel.visonneau@ec-nantes.fr, web page: http://www.ec-nantes.fr

Key words: Computational fluid dynamics, hydrodynamics, validation, assessment, workshop

Summary. The Gothenburg 2010 Workshop on Numerical Hydrodynamics gathered 33 groups with computations for one or more of 18 test cases. All results were collected and discussed at a meeting in Gothenburg in December 2010. In the present paper some representative examples from the workshop are presented. The complete results are found in the workshop Proceedings.

1 INTRODUCTION

In 1980 an international workshop on the numerical prediction of ship viscous flow was held in Gothenburg[1]. The purpose was to assess the state-of-the-art and to find directions for the future developments in the field. Participants in the workshop had been invited long before and had delivered results for two well specified test cases to the organizers. Detailed information on the features of each participating method had also been submitted and compiled in a table. By comparing the computed results on the one hand, and the details of the methods on the other, the most promising approaches could be sorted out.

Now, more than 30 years have passed since this first workshop and the event has been repeated a number of times. In 1990 the second workshop was held, again in Gothenburg[2]. While practically all methods participating in the 1980 workshop had been of the boundary layer type, now all but one were of the RANS type. A huge improvement in the prediction of the flow around the stern was noted. The workshop idea was picked up in Japan in 1994 and

the third workshop was held in Tokyo in 1994[3]. Notable from this workshop is that free-surface capabilities had become available in many of the methods. The fourth workshop in the series was held in Gothenburg in 2000[4,5]. Now, three modern hull forms were introduced as test cases, and these hulls have been kept ever since. At this time formal verification and validation (V&V) procedures were introduced. While in the previous workshops the emphasis had been on the wake and waves for a towed hull, self-propulsion was introduced in 2000. This was kept in the fifth workshop in Tokyo in 2005[6], where some sea-keeping and manoeuvring cases were introduced as well. Even though the same three hulls were used this increased the number of test cases significantly. A further step in this direction was taken at the most recent workshop, held in Gothenburg in December of 2010. This workshop is the topic of the present paper.

2 HULLS

The three hulls used in the workshop were:

1) The KVLCC2, a second variant of a Korean VLCC
2) The KCS, a Korean container ship
3) The DTMB 5415, a US combatant

The KVLCC2 was designed at the Korea Research Institute for Ships and Ocean Engineering (now MOERI) around 1997 to be used as a test case for CFD predictions. Extensive towing tank tests were carried out, providing data for resistance, sinkage and trim, wave pattern and nominal wake at several cross-planes near the stern[7,8,9]. Mean velocity and turbulence data were obtained by Postech[10] in a wind tunnel. At the CFD Tokyo Workshop in 2005[6] there was a slight modification of the stern contour of this ship and it was therefore renamed as KVLCC2M. The modification is explained in Hino[6]. In the present workshop the original design was used.

Also the KCS was designed by MOERI for the same purpose as the KVLCC2, and similar tests were carried out for this hull[7,8,9]. Self-propulsion tests were carried out at the Ship Research Institute (now NMRI) in Tokyo and are reported in Hino[6]. Data for pitch, heave, and added resistance are also available from Force/DMI measurements[11].

Model 5415 was conceived as a preliminary design for a Navy surface combatant around 1980. The hull geometry includes both a sonar dome and a transom stern. Propulsion is provided through twin open-water propellers driven by shafts supported by struts.

The model test data for the 5415 includes:

- Local flow measurements (Mean velocity and cross flow vectors)[12].
- PIV-measured nominal wake in regular head waves (Mean velocity, turbulent kinetic energy, and Reynolds stresses)[13].
- Resistance, sinkage, trim, and wave profiles[12].
- Wave diffraction (Waves, 1st harmonic amplitude of mean velocities, turbulent kinetic energy, and Reynolds stresses)[13, 6].
- Roll decay (Motion, free surface, mean velocities)[14].

Side views of the three hulls are seen in Figure 1 and the main particulars are given in Table 1. No full scale ships exist.

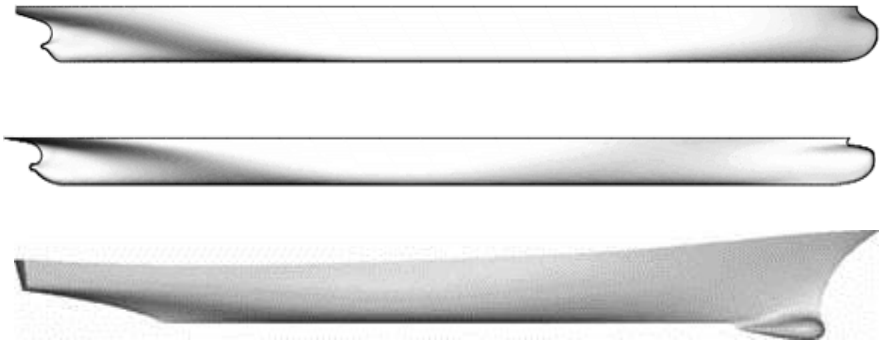

Figure 1: The three ships used in the workshop (upper : KVLCC2; middle : KCS; bottom : 5415)

Main Particulars (Full Scale)			KVLCC2	KCS	DTMB 5415
Length between perpendiculars		L_{PP} (m)	320.0	230.0	142.0
Maximum beam of waterline		B (m)	58.0	32.2	19.06
Draft		T (m)	20.8	10.8	6.15
Displacement		Δ (m^3)	312622	52030	8424.4
Wetted area w/o rudder		S_W (m^2)	27194	9424	2972.6
Wetted surface area of rudder		S_R (m^2)	273.3	115.0	30.8
Block coefficient (C_B)		$\Delta/(L_{PP} \cdot B \cdot T)$	0.8098	0.6505	0.507
Service speed	Speed	U (knots)	15.5	24.0	18.0, 30.0
	Froude number	Fr	0.142	0.26	0.248, 0.413

Table 1 : Main particulars of the three ships

3 TEST CASES

Several types of computations were requested, namely:

1) Local flow at fixed condition, either zero sinkage and trim (denoted FX_0) or dynamic sinkage and trim ($FX_{\sigma\tau}$)
2) Resistance, sinkage and trim either at FX_0 or at heave- and pitch-free condition ($FR_{z\theta}$)
3) Self-propulsion at FX_0 or $FR_{z\theta}$
4) Heave and pitch in waves either at $FR_{z\theta}$ or with free surge ($FR_{xz\theta}$)
5) Forward speed diffraction at $FX_{\sigma\tau}$
6) Free roll decay at $FX_{\sigma\tau}$ and free to roll (FR_{φ})

Note that maneuvering was not included, since it was the topic of the recently held SIMMAN workshop in the spring of 2008[15].

All test cases for the three hulls are listed in Table 2. The measurements were taken at the organizations within brackets. See the references above. There are altogether 18 cases and the participants were free to select which cases to compute.

4 PARTICIPANTS AND METHODS

The workshop participants are listed in Table 3, together with the main features of their methods. In the first column the acronym of the participating group is given. This is used

Case Number	Hull	Attitude	Measured quantity
1.1a	KVLCC2	FX_0	Mean velocity, Reynolds stresses (Postech WT)
1.1b		FX_0	Wave pattern (MOERI)
1.2a		FX_0	Resistance (MOERI)
1.2b		$FR_{z\theta}$	Resistance, sinkage and trim (MOERI)
1.4a		$FR_{z\theta}$	Pitch, heave, added resistance (INSEAN)
1.4b		$FR_{z\theta}$	Pitch, heave, added resistance (NTNU)
1.4c		$FR_{xz\theta}$	Surge, Pitch, heave, added resistance (Osaka Univ)
2.1	KCS	FX_0	Wave pattern, mean velocities (MOERI)
2.2a		FX_0	Resistance (MOERI)
2.2b		$FR_{z\theta}$	Resistance, sinkage and trim (MOERI)
2.3a		FX_0	Self propulsion at ship point (thrust, torque, force balance or RPM, mean velocity), local flow (NMRI)
2.3b		$FR_{z\theta}$	Self propulsion at model point (thrust, torque, force balance or RPM), sinkage and trim (FORCE)
2.4		$FR_{z\theta}$	Pitch, heave, added resistance (FORCE)
3.1a	DTMB 5415	$FX_{\sigma\tau}$	Mean velocity, resistance, wave pattern (INSEAN)
3.1b		$FX_{\sigma\tau}$	Mean velocity, resistance, wave pattern, Reynolds stresses (IIHR)
3.2		$FR_{z\theta}$	Resistance, sinkage and trim (INSEAN)
3.5		$FX_{\sigma\tau}$	Wave diffraction, Mean velocity (IIHR)
3.6		FR_{φ}	Roll decay (IIHR)

Table 2 : Test cases

in combination with the code name of column three to identify each submission. The cases computed are given in column two. In the remaining columns the features of each method are given.

The majority of methods use two-equation turbulence models, k-ε or k-ω. There are also some one-equation models, Spalart-Allmaras or Menter. The anisotropic models are either of the algebraic stress or Reynolds stress type. Note that there are also some LES/DES methods and even a DNS method. Most of the participants use no-slip wall boundary conditions, but there are also several methods with wall functions, both with and without pressure gradient corrections. The Volume of Fluid (VOF) technique is the most popular one for the free-surface modeling, followed by the level set methods. There are only three entries with surface tracking. The propeller is represented either as an actual rotating propeller or through a body force approximation. Simulations were performed using both finite difference and finite volume codes, but there was no finite element method. 2nd or 3rd order accurate schemes were used and limited studies used 4th order schemes. Most methods are pressure based, but there are also several solving the equations directly or with an artificial compressibility.

The grids used were either single- or multi-block structured (butt-joined or overlapping) or unstructured. There was a huge variation in grid density, from 0.3M to 300M. Most of the

Table 3(1) : Workshop participants and methods

Organization	Cases Submitted	Code	Turbulence (incl. non-RANS)	Wall Model	Free Surface	Propeller	Discretization		Grid Type	Velocity Pressure
							Type	Order		
CD-Adapco	2.2a, 2.2b	STAR-CCM+	Standard k-ε	N	VOF	-	FV	2	U	PR
CEHINAV TU Madrid	3.1a	STAR-CCM+	k-ω SST	N	VOF	-	FV	1	MU	PR SIMPLE
Chalmers	1.1a	SHIPFLOW4.3	k-ω SST EASM	N	-	-	FV	2	S	A
CSSRC	2.1, 2.2a, 2.2b, 2.3a, 3.1a, 3.2	FLUENT 6.3	k-ω SST RNG k-ε	N	VOF	Actual	FV	2	MS	PR SIMPLE
CTO	2.3a	STAR-CCM+	k-ε	N WO	VOF	Actual	FV	2	U	PR SIMPLE
ECN/CNRS	1.1b, 1.4a, 1.4b, 3.6	ISISCFD	k-ω, EASM	WO	VOF	Body force	FV	2	U	PR SIMPLE
ECN/HOE	1.1a, 1.1b, 1.4a, 1.4b, 2.1, 3.1a, 3.1b, 3.5, 3.6	ICARE	Wilcox k-ω k-ω SST	N WO	Nonlin. track	Body force	FD	2	S	DM
FLOWTECH	2.1	SHIPFLOW-VOF-4.3	k-ω SST	N	VOF	-	FV	2	MS	A
FOI	3.1a	OF	LES	WO	VOF	-	FV	2	U	PR
FORCE	2.4	CFDShip-Iowa	k-ω SST	N	Level set	-	FD	2	OS	PR PISO
GL&UDE Univ. Duisburg	1.4a, 1.4b, 1.4c, 2.2a, 2.2b, 2.4, 3.6	Comet OpenFOAM	k-ε	N WO	VOF	-	FV	Mixed	U	PR SIMPLE
HSVA	1.1a, 1.2a	FreSCo+	2E k-ω	N	VOF	-	FV	3	U	PR
IHI/Univ. Tokyo	2.4	WISDAM-UTokyo	Baldwin-Lomax and DSGS	N	Density function ρ	-	FV	3	OS	PR MAC
IIHR	1.1a, 1.4a, 1.4c, 2.1, 2.3a, 2.3b, 2.4, 3.1a, 3.1b, 3.5, 3.6	CFDShip-Iowa V4, V4.5, V6	Hybrid k-ε/k-ω based DES Hybrid ARS based DES	WO N	Level set	Actual Body force	FD	2~4	S, OS	PR Fractional step
IIHR-SJTU	2.1, 2.3a	FLUENT12.0.16	Realizable k-ε	N, W	VOF	Body force	FV	3	MS	PR
IST	1.1a	PARNASSOS	k-ω SST	N	-	-	FD	2	S	DM
Kyushu University	1.4b	RIAM-CMEN	DNS	N	THINC	-	FD	3	S	PR

Table 3(2) : Workshop participants and methods

Organization	Cases Submitted	Code	Turb. model (incl. non-RANS)	Wall Model	Free Surface	Propeller	Discretization		Grid Type	Velocity Pressure
							Type	Order		
MARIC	1.1a, 1.1b, 1.2a, 2.1, 2.2a, 2.3a, 3.1a, 3.1b, 3.2	FLUENT	Realizable *k-ε*	N	VOF	Actual	FV	2	MS	PR SIMPLE
MARIN	2.1, 2.3a, 3.1a, 3.2	PARNASSOS	1E Menter	N	Free-surface fitting	-	FD	2	MS	DM
MOERI	1.1b, 1.2a, 1.2b, 2.1, 2.2a, 2.2b, 2.3a, 2.3b	WAVIS	Realizable *k-ε*	WO	Level set	Body force	FV	3	MS	PR SIMPLEC
NavyFOAM (NSWC/P S ARL)	1.1a, 3.1a, 3.1b, 3.2	NavyFOAM	Wilcox *k-ω*	WO	VOF	-	FV	2, 3	MS MU	PR
NMRI	1.1a, 2.1, 2.3a, 3.1b, 3.5	SURF	1E Modified Spalart-Allmaras	N	Level set	Body force	FV	2	S, U	A
NSWC-PC ARL	3.2	CFDShip-Iowa V4.5	DES Hybrid *k-ε*/*k-ω*	N	Level set	-	FD	4	S, OS	PR
NTNU	1.1a, 1.1b, 1.2a	FLUENT	*k-ω* SST	N	VOF	-	FV	2	MU	PR SIMPLE
SNUTT	2.1, 2.3a	FLUENT6.3	*k-ε*	W	VOF	Actual	FV	2	MU	DM
Southampton Univ. QinetiQ	2.1, 2.2b, 2.3a	CFX 12	*k-ω* SST	W	VOF	Body force	FV	2	MS	DM
SSPA	2.3a, 2.3b	SHIPFLOW4.3	EASM	N	-	Body force	FV	2	OS	A
SSRC Univ. Strathclyde	2.1, 2.3a, 3.1b, 3.5, 3.6	FLUENT12.1	*k-ω* SST	N	VOF	Actual	FV	2	MS	PR
SVA Potsdam	2.1, 2.2a	ANSYS-CFX12	*k-ω* SST	N	VOF	-	FV	2	MU	DM
TUHH	1.1b, 2.4	FreSCo+	*k-ω* SST	N	VOF	-	FV	3	U	PR SIMPLE
TUHH ANSYS	2.1, 2.2a, 2.3a,	CFX12.1	*k-ω* SST	N WO	VOF	Actual	FV	2	MS	Fully coupled *w-p*, SIMPLER *p*-equation
Univ. Genova	3.1a, 3.2	StarCCM+	Realizable *k-ε*	N	VOF	-	FV	2	U	PR SIMPLE
VTT	1.1a, 1.1b, 1.2a, 2.1	FINFLO	*k-ω* SST	N	Nonlin. track	-	FV FD	3	MS OS	A, PR

A-Artificial compressibility; DM-Direct method; FD-Finite difference; FV-Finite volume; MS-Multiblock structured; MU-Multiblock unstructured; N-No slip; OS-Overlapping structure; PR-Pressure correction; S-Single block structured; U-Unstructured; W/WO-Wall functions with/without pressure gradient correction

simulations were performed with grids in the range 1-10M, but some resistance and self-propulsion cases had grids up to 24M cells. There were also a few submissions from IIHR with grids around 300M.

5 SELECTED RESULTS

The Workshop Proceedings[16] contain 380 pages of tables and diagrams displaying the submitted results. Also included in the Proceedings are three evaluation reports written by the organizers. These reports contain altogether 125 pages of discussions. With the space limitation of the present paper only a few examples from the Proceedings can be given. The examples will be presented by subject (c.f. "Types of computations" in Section 3): resistance, self-propulsion, wave pattern, local flow, heave and pitch, and roll decay. Unfortunately, sinkage and trim, wave diffraction and the very extensive discussions on Verification and Verification (V&V) will have to be left out.

5.1 Resistance

In Table 4 a statistical analysis of all computed total resistance coefficients is presented. While the case and Froude number are presented in columns 1-3, column 4 gives the mean comparison error E_{mean} in per cent of the measured data value, D. According to the sign convention of the Workshop E_{mean} is defined as $D - S_{mean}$, where S_{mean} is the mean of all simulated values for the particular case. The standard deviation, σ, is given in column 5 in per cent of the data value, and in column 6 the estimated data uncertainty is presented. Finally, in the last column the number of entries for the case is seen. Values within brackets are from the 2005 Workshop[6].

Comparing the 2010 and 2005 results a substantial reduction in the standard deviation (%D) for the towed KVLCC2 and KCS cases is noted, from 6.2 to 1.3 and from 4.2 to 1.2 respectively in the fixed condition. Also, $|E_{mean}|$ for these conditions is well below 2%D, which indicates that all predictions for this condition are quite accurate, although still not within the experimental accuracy. There is only one submission for the free KVLCC2 condition and $|E_{mean}|$ for all Froude numbers is of the same size 2.1%D. The free KCS condition has several submissions and very small comparison errors (0.2%D) and standard deviations, around 1%D for both.

The self-propelled KCS has standard deviations around 3%D and the comparison error is very small for the fixed case. However, for the free case $|E_{mean}|$ is quite high: 7.2%D. All three submissions under predict the resistance significantly. It should be noted that the fixed KCS in self-propulsion is the only case for which the standard deviation has increased compared to 2005.

5415 with sinkage and trim fixed to the dynamic values have comparison errors below 3%D and standard deviations around 4%D. In view of the fact that the only difference between 3.1a and 3.1b is the Reynolds number (apart from a very small difference in sinkage and trim), the difference is large, but the statistical basis is too small for a comparison. For the free 5415 in 3.2 both the mean error and the standard deviation seem to depend strongly on the Froude number. The best results are obtained at $Fr = 0.28$, where the water just clears the transom. For this condition the mean error is practically zero and the standard deviation

among the 6 submissions is 2.1%*D*.

Table 4 shows the statistics for all cases, and indicates the accuracy obtainable for each case. Even more interesting is however the information found on the last line: the mean error and the mean standard deviation (weighted by number of entries) for all cases. The mean error for all computed cases is practically zero; only - 0.1%*D*, while the mean standard deviation is 2.1%*D*; a surprisingly small value. In the 2005 Workshop the mean error of all 40 submissions was in fact equally small: 0.1%*D*, while the mean standard deviation was 4.7%*D*. While the distribution between "simple" and "difficult" cases is not the same in the two Workshops, it seems safe to conclude that the scatter has been reduced considerably. In fact, even the largest standard deviation in the present computations (Cases 3.1b and 3.2) is smaller than the mean standard deviation in 2005.

Hull	Case No.	*Fr*	E_{mean} %*D*	σ %*D*	U_D %*D*	No. of Entries
KVLCC2	**1.2a** (fixed)	0.1423	-1.7 (0.0)	1.3 (6.2)	1.0 (0.7)	5 (13)
	1.2b (free)	0.10~0.15	-2.1	-	1.0	1
KCS	**2.2a** (fixed)	0.26	-1.3 (-1.1)	1.2 (4.2)	1.0	8 (11)
	2.2b (free)	0.11~0.28	-0.2	1.2	1.0	27
	2.3a (fixed, prop.)	0.26	-0.3* (-0.9)	3.1 (1.0)	-	14* (4)
	2.3b (free, prop.)	0.26	7.2	3.3	-	3
5415	**3.1a** (fixed s&t)	0.28	2.5 (1.6)	3.8 (5.3)	0.6 (2.2)	5 (11)
	3.1b (fixed s&t)	0.28	-2.6	4.4	0.6	5
	3.2 (free)	0.138	-2.8	4.4	1.3	5
		0.28	0.1 (-1.9)	2.1 (-)	0.6 (2.2)	6 (1)
		0.41	4.3	1.4	0.6	5
Mean of all cases			E_{mean} = -0.1%*D*	σ_{mean} = 2.1%*D*		89 (40)

Table 4 : Resistance statistics, all cases (*: Results from MARIC with a hub cap are excluded)

Figure 2 shows the comparison errors for all submitted cases versus grid size. For each submission the turbulence model is denoted by a symbol. It is seen that about 90% of all computations are made with grids smaller than 10M cells. The scatter within this range seems to be significantly larger than for the larger grids. However, this is mainly caused by the large scatter of the self-propulsion submissions (represented by filled symbols), so if these are excluded, and only towed resistance is considered, there is no error decrease above 3M grid points. All points seem to be within approximately +- 4%*D*. Not even the very large grid at 300M cells (moved into the figure and marked) shows any significant improvement; it is slightly below 3%*D*. However, below 3M cells the maximum errors increase to about 8 %*D*.

There is a large number of entries for the 2-equation models and the results are generally good. For the others there are rather few entries. The relatively poor result for the more advanced methods is a surprise. However, EASM and RS, ARS suffer from one bad point for a very coarse grid and two bad points computed for the self-propulsion cases, which may be more difficult than the towed cases. The three very good results for the Menter model were obtained with the same code and user. It would be interesting to investigate the performance

of each model in different ranges of grid density, but that has not been done so far.

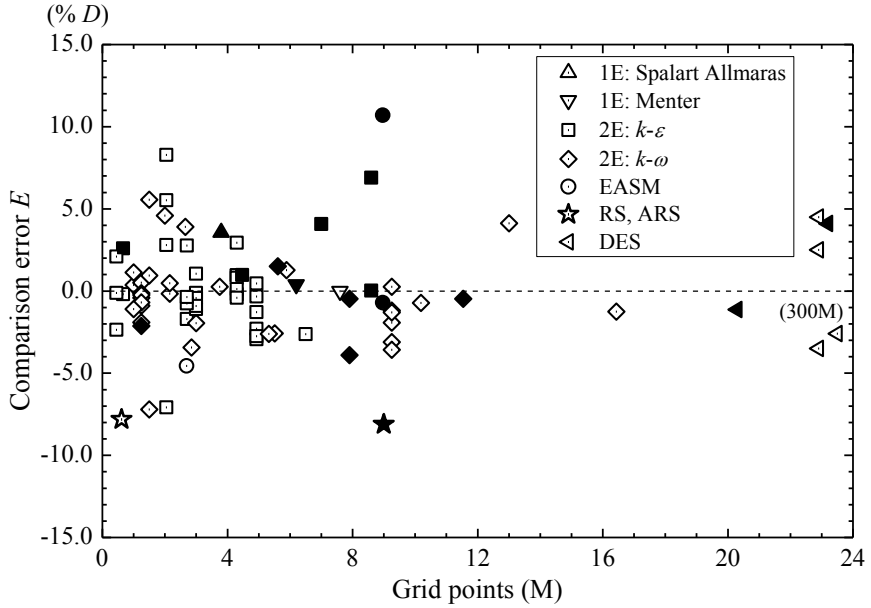

Figure 2: Comparison error of all resistance submissions vs. grid size (turbulence model parameter). Filled symbols represent propulsion cases

5.2 Self-propulsion

Self-propulsion results were requested only for the KCS hull and only at one Froude number: 0.26. In Case 2.3a the hull was kept fixed in the zero speed attitude, while in 2.3b the hull was free to sink and trim. Experimental data are available from NMRI for a 7.3 m hull in 2.3a and from FORCE for a 4.4 m hull in 2.3b. The NMRI hull was without a rudder, while a rudder was fitted to the FORCE hull.

In 2.3a computations were requested for the model at the ship point, i.e. the hull was towed to account for the larger skin friction at model scale compared to full scale. This force, the skin friction correction, *SFC*, was pre-computed and was the same as in the measurements. In the experiments the thrust T, was adjusted by varying the rpm, n, such that $T = R_T(SP)$-SFC, where $R_T(SP)$ is the resistance in self-propulsion. Most of the participants did the simulations in this way, i.e. the force balancing was automatically achieved by the flow code. An alternative was to avoid the balancing and use the measured rpm in the simulation. In the first case the achieved n was requested, while in the second case the resulting towing force $R_T(SP)$-T was to be reported. In 2.3b computations were carried out for the model point, so no towing force was applied, but the balancing was carried out in the same way as in 2.3a.

The dependence on the grid density of the thrust coefficient, K_T, torque coefficient K_Q, achieved n for force balancing and towing force $R_T(SP)$-T for given n are plotted in the Proceedings, but cannot be presented here due to the space limitation. There is a clear difference in scatter between the three predictions in the range 10-24 M cells and those below 10M. For K_T, K_Q and n the maximum scatter in the upper range is around +- 7%, 5% and 2%, respectively, while in the lower range it is within 19%, 18% and 6%. For the towing force

$R_T(SP)$-T there are very few entries and the largest error is for an 11.5M grid. All quantities but n have considerably larger errors than resistance.

Of more interest is perhaps the difference between the actual and modeled propellers and between the force-balanced and fixed rpm cases. Difficulties of handling the free-to-sink-and-trim case may be revealed by comparing 2.3a and 2.3b, so the available set of results may be cut in different directions. To get a quantitative base for these comparisons Table 6 has been prepared. Here actual propeller results may be compared with those from modeled propellers, computations with a given *SFC* with those with a given n, and the fixed attitude results from 2.3a with the free attitude results from 2.3b. The comparisons are made in terms of the mean error E_{mean} and the mean absolute error $|E|_{mean}$, both in per cent of the experimental data. A standard deviation is not meaningful, except in the comparison between 2.3a and 2.3b, since the other comparisons include two cases.

Items (No. Entries / Total)	K_T		K_Q		n		$R_T(SP)$-T	
	E%D mean	*|E%D| mean*	*E%D mean*	*|E%D| mean*	*E%D mean*	*|E%D| mean*	*E%D mean*	*|E%D| mean*
Actual prop. (9/17)	3.3	4.1	-1.4	2.9	-2.1	2.1	-7.8	7.8
Modeled prop. (8/17)	-2.4	6.5	-3.9	8.1	1.6	2.8		
Given *SFC* (12/17)	-0.2	6.0	-2.6	6.5	0.4	2.6		
Given n (5/17)	2.4	3.2	-2.6	2.6	-	-	-7.8	7.8
Case2.3a (14/17)	-0.6	5,0	-4.6	5.1	0.6	2.3	-7.8	7.8
Case2.3b (3/17)	6.2	6.3	6.7	6.7	-0.3	3.6	-	-
Mean (Case 2.3a&b)	0.6	5.2	-2.6	5.4	0.4	2.6	-7.8	7.8
Mean σ (Case 2.3a&b)	7.0		6.0		3.1		8.7	

Table 5 : Error statistics, Cases 2.3a and 2.3b

There is a clear trend of smaller scatter for the actual propellers in K_T, K_Q and n (for $R_T(SP)$-T there are only actual propellers represented). All three quantities have a smaller $|E|_{mean}$ for the actual propellers than for the modeled ones, and the difference is particularly large K_Q. For the mean error E_{mean} there is no clear trend. The actual propeller exhibits a considerably smaller error in K_Q, but for K_T and n the errors are slightly larger.

The scatter in the K_T and K_Q results is quite different between a given towing force and a given rpm. $|E|_{mean}$ for given n is only half of that for given towing force, while the mean signed error E_{mean} is larger for K_T. The most surprising result here is the large over prediction of the towing force for given rpm. If n is given, the towing force is significantly over predicted, while if *SFC* is given (and the forces balanced) the rpm is computed very well (see the relatively small values of E_{mean} and $|E|_{mean}$ for n). If the propeller is relatively lightly loaded a small (percentage) change in n may correspond to a relatively large (percentage) change in trust and a corresponding large change in towing force to acquire force balance.

It is seen in Table 5 that the small number of results for 2.3b (only 3) makes it very difficult to draw conclusions concerning the differences in accuracy between the fixed and free cases. E_{mean} and $|E|_{mean}$ for all quantities have been computed and presented in the table, but we will refrain from drawing any conclusions.

The last two lines of Table 6 are the most interesting ones. They present the mean values of

all self-propulsion submissions, i.e. a weighted average of the results in 2.3a and 2.3b. These numbers may give a general indication of the accuracy obtainable in self-propulsion predictions. The last line gives the weighted mean of the standard deviations in the two cases. For K_T the mean error is 0.6%D and the mean standard deviation 7%D and the corresponding values for K_Q are -2.6%D and 6%D, respectively. The predicted n for a given SFC has a mean error of 0.4%D and a standard deviation of 3.1%D, while the numbers are larger for the towing force for given n: -7.8%D and 8.7%D, respectively.

5.3 Wave pattern

Wave pattern predictions were reported for Cases 1.1b (KVLCC2), 2.1 (KCS) and 3.1a, b (5415). The hulls represent completely different ship types and Froude numbers, so the capability of the codes to predict the free surface was tested over a wide range of possibilities. Several different graphs were used to evaluate the performance of the codes. A general overview was provided in the wave contour plots, where the wave height was given in a region surrounding the hull. Wave cuts at three distances from the center plane were also presented for all hulls. These cuts enabled a very detailed comparison between computed and measured waves, since the measured data were presented in every plot.

Since the predicted waves are strongly dependent on the grid density near the surface every participant was requested to provide the following grid information: number of grid points per fundamental wave length along the waterline, number of grid points in the transverse direction on the surface at midship and step size in the vertical direction near the hull at midship. This information was plotted in a graph that is presented after the wave figures for each case in the Proceedings.

Due to the space limitation only one example will be given here, namely the most challenging one: Case 1.1b. The Froude number for KVLCC2 is quite low, 0.142, which means that the fundamental wave length $2\pi Fr^2$ is only 1/8 L_{PP}, so a large number of cells are required to get a sufficient number of cells per wave length. Small cells are also required in the vertical direction, since the maximum wave height is less than 1% L_{PP}.

Wave contours for KVLCC2 are presented in Figure 3. The measurements by MOERI reveal a complex wave pattern with very short waves essentially located at the edge of the Kelvin wedge. For a hull of this type with pronounced shoulders four wave systems should be expected: one from the high pressure regions at each end of the hull and one for each shoulder. However, the speed is so low in this case that no waves seem to be generated near the stern. The dominating wave system is that from the bow, but close inspection also reveals a more weak system originating at the forward shoulder and merging with the bow system after a short distance.

The best results were obtained by ECN/CNRS-ISISCFD, which is an unstructured grid solver with surface capturing and the VOF technique. The results, as seen in Figure 3, reveal all the details of the wave pattern. In fact, the computations display the generated shoulder wave system more clearly than the experiments. It is seen inside the main system from the bow and merges with the latter around x/L_{PP}=0.75. ISISCFD has a newly implemented grid adaptation technique where the original grid is refined in several steps and concentrated in regions where a large grid density is required. The total number of grid points was 5.5M, but

grid convergence was reported even with 2.7M grid points. The grid density plot (not shown here) shows that along the hull the step size has two peaks, like in most grid plots, one at the bow and one at the stern. In this case the maximum grid density at the bow is around 200 points per wave length (ppwl), while at the stern the density is somewhat lower, around 150 ppwl. Along the main part of the hull the density is around 70 ppwl. There is an interesting variation in the grid density in the transverse direction. Like in all methods the transverse grid density is very large close to the hull, in order to resolve the boundary layer, so there is first a rapid drop in ppwl, moving outwards. In most methods this drop is gradually reduced and a relatively smooth curve is obtained from the hull towards the outer edge of the free surface domain. However, in this case the adaptivity created a peak in the region y/L_{PP}= 0.15-0.25. This is where the bow wave system passes x=0, where the grid density is reported. In the vertical direction the step size was reduced to about $3\times10^{-4}L_{PP}$ close to the surface, which corresponds to about 20 cells per maximum wave height.

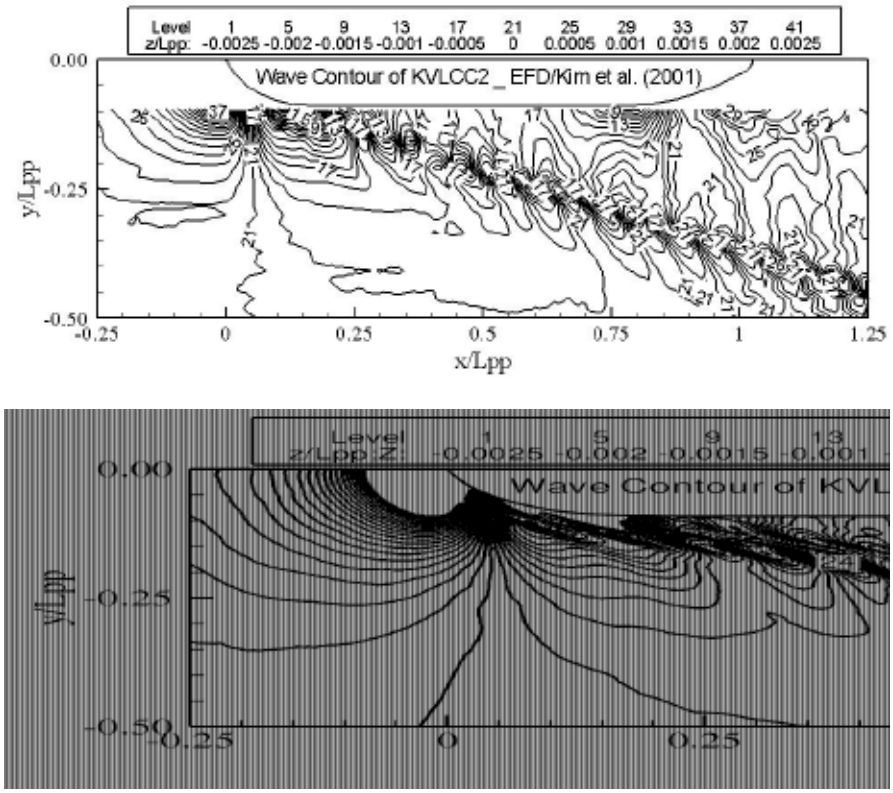

Figure 3: Wave pattern around the KVLCC2 at Fr=0.142.
Top : measurements from MOERI, bottom : computations by ECN/CNRS-ISISCFD

5.4 Local flow (steady case)

A large number of local flow results were requested at the Workshop. Contours of axial velocity and cross-flow vectors were to be provided for all three hulls both under steady (all hulls) and unsteady (5415) conditions, even with an operating propeller (KCS). This information was requested for one or more cross-planes. Velocity profiles in the propeller

plane were also asked for. Turbulence data at the propeller plane were requested for KVLCC2 and 5415. For KVLCC2, wake fraction contours and limiting streamlines were to be reported and surface pressure distributions should be given for KVLCC2 and KCS.

Here only one example can be given, and to be able to compare with previous workshops we select the flow at the propeller plane of the KVLCC2. The flow at model scale around this hull is characterized by the gradual development of an intense stern bilge vortex which creates a strong distortion of the axial velocity iso-contours at the propeller plane. See Figure 4. This distortion is due to the transport of low momentum fluid from the vicinity of the hull to the center of the flow field under the action of the longitudinal vortex. Under the main vortex, one can guess the existence of a secondary counter-rotating vortex close to the vertical plane of symmetry. This leads to the so-called hook-shape of the iso-wakes which is clearly visible both in the towing tank experiments from MOERI and wind tunnel experiments from Postech. In Figure 4 the Postech results are presented. There is however a difference between the two results particularly in the vicinity of the vertical plane of symmetry (the level U=0.4). These local differences may be attributed to blockage effects, the tunnel blockage being more than 6% while the towing tank blockage is only 0.3%. On the other hand, it seems easier to control the quality of the measurements (in terms of flow symmetry for instance) in a wind tunnel than in a towing tank where small free-surface deformations may create perturbations. These various sources of experimental errors will have to be considered during the comparisons with computations which were performed without any blockage effect and free-surface deformation. It should also be mentioned that the hull geometry provided for the G2010 workshop is slightly different from the original KVLCC2 since a semi-hemispherical cap (dummy hub) has been placed at the end of the hub to make the flow around the shaft center line smooth.

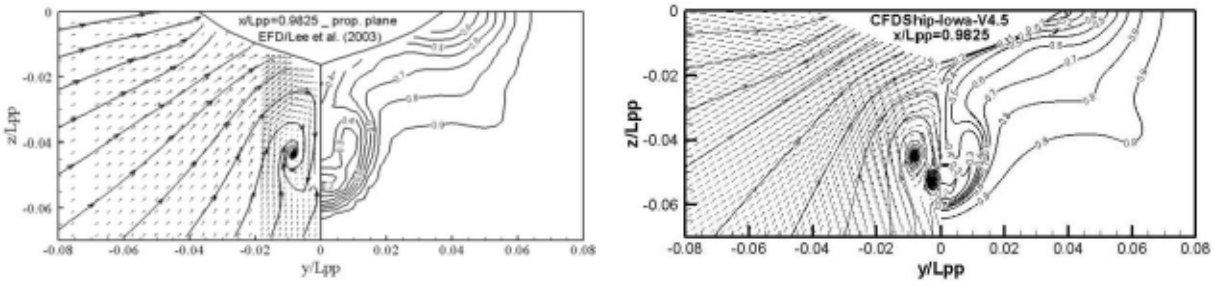

(a) (b)

Figure 4: Cross-flow vectors, 2D 'streamlines'and axial velocity contours at the propeller plane of the KVLCC2. (a) Measurements at Postech[9] ; (b) Computations by IIHR-CFDShip Iowa-V.4.5 (ARS)

At the propeller plane the bilge vortex has developed and its impact on the iso-wakes is very large. A first group of results is in very good agreement with experiments, namely IIHR/CFDShip-Iowa-V4.5 (ARS, DES), NTNU/FLUENT, NMRI/SURF, Chalmers/SHIPFLOW4.3, MARIC/FLUENT6.3 and NavyFOAM/NavyFOAM. The IIHR/CFDShip-Iowa-V4.5 (ARS) results are displayed in Figure 5. Except NavyFoam/NavyFoam which uses a k-ω model (original version of 1998 according to their paper), all other results are based on various anisotropic turbulence models. IIHR/CFDShip-Iowa-V4.5 used both an algebraic Reynolds Stress model (ARS) and an ARS based DES

version while both Chalmers/SHIPFLOW4.3 and NMRI/SURF use the Explicit Algebraic Stress Model developed by ECN-CNRS some years ago. Computations performed with FLUENT (NTNU/FLUENT and MARIC/FLUENT6.3) are based on a more complex Reynolds Stress Transport Model which solves additional transport equations for the Reynolds Stress components. It is interesting to notice that all these results agree better with the towing tank than with the wind-tunnel experiments. The main stern bilge vortex is very accurately captured and the hook-shape of the iso axial velocity contours is very well reproduced. A second counter-rotating vortex, hardly visible in the experiments, is present in all these computations. In that region, the agreement between the best solutions and the experiments is less good. Let us recall that this is a region where the flow is probably influenced by the shape of the hub which is slightly different because of the presence of the hub cap in the computations. One can also notice that the ARS based DES solution contains more intense longitudinal vortices, a characteristic already observed in other test cases (Case 3.1a for instance).

On the other hand, linear eddy viscosity models without ad-hoc rotation correction under-estimate the intensity of the bilge vortex (ECN-BEC/Icare, HSVA/FreSCo+, IST-MARIN/PARNASSOS-SST, VTT/FINFLO). A noticeable exception is NavyFoam, based on the Wilcox's k-ω 1998 model, which gives a prediction similar to that obtained with algebraic Reynolds stress model. As this model is not as widely used as the SST model for example, and this peculiar performance needs to be further validated by other flow solvers. IST/MARIN presents some good predictions for the nominal velocity obtained with linear eddy-viscosity model with rotation correction or with a linear turbulence model. The improvement obtained by those ad-hoc modifications seems to be limited only to the mean velocity field at propeller plane. In particular, the recirculation region seems to be extended more upstream.

It is well known that turbulence anisotropy is an additional source of longitudinal vorticity production. In fact the turbulence anisotropy acts as a direct source term in the transport equation of the longitudinal vorticity. Having the normal Reynolds stresses available at the propeller plane makes possible a detailed verification of the amount of measured anisotropy in the plane. If one compares the relative values of the normal turbulent stresses, one can notice a strong anisotropy inside the characteristic hook shape found in the iso-axial velocity contours. For instance, max(uu)=0.016, max(vv)=0.007 and max(ww)=0.008 while max(k)=0.016. Most of the codes using explicit anisotropic turbulence models are able to predict with a reasonable agreement the turbulence structure at this cross-section. For instance, NMRI/SURF finds max(uu)=0.014, max(vv)=0.008 and max(ww)=0.010. The relative weights of the respective normal turbulent stresses are correctly predicted by DES, RSTM and EASM turbulence models while the linear isotropic models fail to reproduce the measured turbulence characteristics. Therefore, instead of using the right mechanism to enhance the longitudinal vorticity production, correction factors are used to limit the production of turbulence and consequently, to reduce locally the level of turbulent viscosity. This is illustrated by comparing the normal turbulent stresses computed by IST-MARIN/PARNASSOS(SST) to IST-MARIN/PARNASSOS(RCSST), for instance. One cannot see any significant difference on the normal turbulent stresses while the iso axial velocity contours differ. If one compares also the turbulent normal stresses predicted by the

Reynolds Stress Transport model implemented in Fluent, one can notice a remarkable agreement between NTNU/FLUENT and MARIC/FLUENT6.3. Both organizations found max(*uu*) around 0.01, max(*vv*) around 0.004 and max*(ww*) around 0.005, results which are consistently smaller than the experiments. This is again an illustration of a consistent trend associated to a specific turbulence modeling, independently from the grid (which has to be fine enough) and from the user of the solver (who has to be experienced enough...).

This is also the first time that DES results are available for the KVLCC2. The spatial distribution of *uu* is organized around two peaks of *uu* with maximum values around 0.02, greater than the measurements supposed to be around 0.016. The same structure in two peaks is observed for *vv* and *ww* with maximum values around 0.003 and 0.004, respectively. The turbulence anisotropy is therefore more pronounced than what is observed with the anisotropic non-linear turbulence closures. This is probably related with the more pronounced longitudinal vorticity which is found in the DES computations. Although the boundary delimitating full RANSE and full LES formulations is not known, one can suspect that this effect is due to the LES formulations by comparing with the normal turbulent stress distribution obtained with the ARS model.

The turbulent shear stresses *uv* and *uw* were also measured and can be used to perform a detailed assessment of the computations. The agreement of all the computations is reasonable for *uv* except for the DES computations which again do not reproduce the measured spatial distribution. For *uw*, most of the contributors find a zone of $uw > 0.002$ which is consistently smaller than what is observed in the experiments, except the DES closure implemented in CFDShip-Iowa which is in good agreement with the experiments.

Compared to the situations in 2000 and 2005, one can observe that much progress has been made towards consistent and more reliable computations of afterbody flows for U-shaped hulls. The intense bilge vortex and its related action on the velocity field is accurately reproduced by a majority of contributors employing very similar turbulence models implemented in different solvers and on different grids. The debate on the relative importance of discretization vs. modeling errors opened in the mid-nineties should now be closed by the acknowledged prominent role played by turbulence anisotropy as long as a reasonable grid is used. From that point of view, around 3 million points are enough to assess the turbulence closures without any significant pollution from discretization errors. The turbulence data confirm that the turbulence anisotropy is large in the propeller disk and more specifically in the core of the bilge vortex. Explicit Algebraic Stress and Algebraic Reynolds Stress Models reproduce satisfactorily the measured structure of the turbulence and appear to be, up to now, the best answer in terms of robustness and computational cost for this specific flow field, compared to RSTM or DES strategies. Having recourse to Delayed DES will probably strongly improve the present DES results. A more detailed analysis of the turbulence characteristics remains to be done through the use of the Reynolds stress anisotropy tensor, anisotropy invariant maps and the analysis of the turbulent kinetic energy budget.

5.5 Heave and pitch

Several seakeeping cases were included in the workshop. Test cases 1.4a,b and 2.4 are for pitch and heave in regular head waves for KVLCC2 and KCS, restrained in surge. In test case

1.4c for KVLCC2 the surge is also released. Test case 3.5 is forward speed diffraction for 5415 fixed at dynamic sinkage and trim, while Case 3.6 is free roll decay for 5415 at the same attitude. These test cases have not been included in previous CFD Workshops, except test case 3.5, which was included at CFD Workshop Tokyo 2005.

New model tests were conducted for KVLCC2, without appendages, rudders, and propellers. The tests were carried out for all three 1.4 cases (a,b,c). The free surge tests were conducted in the Osaka University's towing tank for a 1/100 scaled model (L_{PP}=3.2 m) using a spring to attach the model to the towing carriage. Fixed surge tests were conducted with the same model in the INSEAN 220×9×3.5 m towing tank and for a larger model (L_{PP} =5.5172 m) at NTNU.

For Case 1.4a-c calm water, four experimental data sets are available which show different values for resistance, sinkage, and trim. Unfortunately, uncertainty of the data was not studied so the origin of the differences cannot be assessed. For the heaving and pitching motions the surge, neglected in 1.4a and b, may be important, since data for surge motion shows that its amplitude increases with wavelength, reaching up to 50% of the wave amplitude for the range of wavelengths tested. For Case 1.4a, there was no phase reference recorded for the data, so phases are not used for CFD error studies. Also, for test case 1.4b the surge motion was partially constrained by a spring system, and as a result the measured resistance amplitude is not used for comparison.

The CFD simulations of cases1.4a-c included 12 submissions from 5 institutions with the number of grid points of 0.3-4.7 M. Verification studies were performed by one submission for Case 1.4a in calm water and waves. The quantities with no higher order effects including steady resistance, 0th harmonic of resistance, and 1st harmonic of motions had minimum prediction errors for all cases. CFD achieved the prediction of 1st order and higher order quantities in the average level of 16%D and 59%D, respectively. For steady and 0th harmonic of resistance, the average error was 17.5%D while the 1st harmonic amplitude and phase were 41%D and 6.5%D, respectively. For motions, the prediction error was 66%D for steady and 0th harmonic while it was around 11%D for 1th harmonic amplitude and 28%D for 1st harmonic phase. Therefore, for resistance, the largest error values were observed for the 1st amplitude, followed by 0th amplitude and then 1st phase. For both heave and pitch motions, the largest error values were observed for the 0th amplitudes followed by 1st phase and 1st amplitude.

The number of grid points seems to have an obvious effect on both motions and resistance results. For most conditions, the smallest errors were for the submission with largest number of points. The other submissions were usually with higher errors based on how coarse their grids are. It may be that all codes would reach the small level of error, if using the finest grid. The smallest error averaged over amplitudes and phase for resistance was 11.19%D for Case 1.4c with λ/L_{PP} =1.1 for CFDShip-Iowa with 4.7M grid points. Also the smallest error averaged over amplitudes and phase for motions was 12.88%D for Case 1.4c with λ/L_{PP} =1.1 for CFDShip-Iowa with 4.7M grid points.

5.6 Roll decay at forward speed

The model-scale test for 1/46.6 scale 5415 bare hull with bilge keels free to roll-decay

advancing in calm water was performed in the IIHR towing tank[13].The flow conditions were Re= 2.56×10^6, Fr=0.138, sinkage = 2.93×10^{-4} L_{PP}, trim = -3.47×10^{-2} degrees and initial roll angle ϕ= 10 degrees. Data were procured for the forces and moments using a strain gage load cell, the unsteady ship roll motion using a Krypton Motion Tracker, the unsteady wave elevation on the starboard side using four servo wave probes, and unsteady velocities at x/L_{PP} = 0.675 in a region near bilge keels using a 2D PIV system.

Four organizations (ECN-ICARE, ECN/CNRS-ISISCFD, GL&UDE-OpenFOAM, and SSRC/Univ of Strathclyde-Fluent 12.2) contributed for this test case, all using URANS methods. All the submissions showed non-linear oscillations for the total resistance as observed in the experiments. The mean resistance was predicted within 10%D of the experimental data. The amplitude and period of the roll motions were predicted very well within 0.85%D as shown in Figure 5.

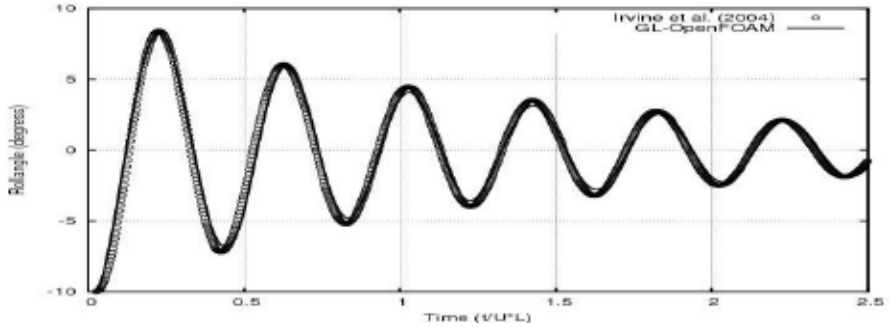

Figure 5: Time history of roll angle
(open circle: experiments; solid black line: CFD (GL&UDE-OpenFOAM))

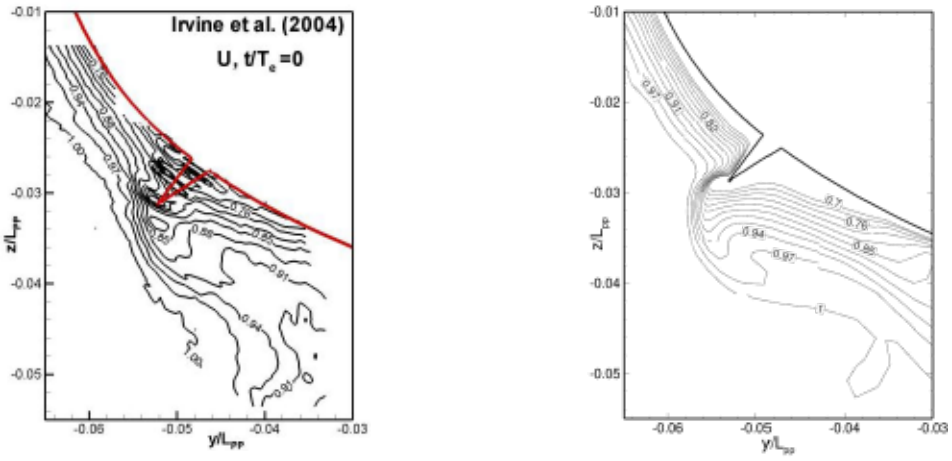

(a) (b)

Figure 6: Contours of U velocity at x/L_{PP} = 0.675 during second cycle of roll decay (t/Te = 0)
(a) Experiment (IIHR, Irvine et al. 2004); (b) Computations by ECN/CNRS-ISISCFD

The ECN-ICARE simulation on a 0.8M grid failed to predict the Kelvin wave pattern and the development of the wave troughs and crests due to the roll motion. Likewise, the SSRC/Univ of Strathclyde-Fluent 12.2 predictions on a 3M grid also showed poor Kelvin

wave predictions, and this was claimed to be due to grid resolution issues.

On the other hand, the ECN/CNRS-ISISCFD predictions on 4.9M grid showed overall good agreement for the Kelvin wave pattern and the development of wave troughs and crest at the shoulder, but the waves were closer to the hull compared to the data and dissipated away from the hull. Overall, the wave elevation predictions improved with grid resolution, but for such low *Fr* (which exhibits a small Kelvin wavelength) even larger grids are required to accurately predict the wave elevation pattern.

The coarse grid ECN-ICARE simulation over-predicted the boundary layer thickness and under-predicted the cross flow velocities by 30%*D*. However the general trends in the cross-flow pattern at the different roll phases were well predicted. This suggests that the generation of the bilge keel vortices was predicted well, but the vortex strengths were under-predicted and significantly diffused compared to the experimental data. ECN/CNRS-ISISCFD predictions on a finer grid compared very well with the experiments, where the minimum and maximum velocities compared within 6% *D*, see Figure 6. The cross-flow predictions were slightly better than the axial velocity, where latter showed over-prediction of the transport of low momentum fluid away from the bilge keel. This suggests that the vortex advection due to roll motion was predicted well, but the bilge keel vortex inception was not predicted accurately. Even finer grids near the bilge keel are required to capture the vortex inception accurately.

Overall, the results showed that the force and roll motion predictions are not significantly dependent on a large resolution, but it is more important for the wave elevation and flow predictions. A further point to note is that the anisotropic turbulence models do not show significant improvement over the isotropic models for the global variable predictions. This is because the vortex generation is imposed by the geometry of the bilge keels, and thus the turbulence models do not influence the flow predictions. This is different from the KVLCC2 test case 1.1a or 5415 test cases 3.1 and 3.5, where the vortices are advected and the anisotropic turbulence models show improved predictions.

6 CONCLUSIONS

The Gothenburg 2010 Workshop on numerical Ship Hydrodynamics was huge effort by a large number of people. 33 groups participated and computed one or more of the 18 test cases for the three hulls. The results represent the state-of-the-art in computational hydrodynamics at present. For the areas covered in the present paper the main conclusions are:

- The mean error (data(*D*) – simulation) for all computed resistance cases was practically zero; only - 0.1%*D*, and the mean standard deviation was 2.1%*D*. The latter represents a considerable improvement since 2005, where the mean standard deviation was 4.7%*D*.
- Of the reported self-propulsion predictions 9 used an actual rotating propeller, while 8 used a hybrid approach with a potential flow propeller model linked to the viscous method. The scatter between the former predictions was roughly half of that of the latter, while the mean error was about the same. The total mean error for K_T and K_Q was 0.6%*D* and -2.6%*D*, respectively, while the mean standard deviation was 7.0%*D* and 6.0%*D*, respectively.

- Very accurate predictions of the wave pattern over the entire discretized free surface were obtained in the most accurate solutions for all three hulls. Even for the most challenging case, at Fr=0.142, all details of the wave pattern were captured by a method with adaptive gridding.
- The details of the nominal wake of the tanker hull could be predicted very well with methods using anisotropic turbulence models. This was true both for mean velocity and turbulence. The mean velocity distribution could also be captured with isotropic models with rotation correction, but with an erroneous distribution between the normal Reynolds stresses. DES seemed to over-predict the anisotropy, thereby exaggerating the bilge vortex strength and the "hooks" in the wake contours.
- Three new sets of data were provided for the workshop in the seakeeping area. The tanker was tested in head waves free in pitch and heave at two organizations and free also in surge at a third laboratory.
- A Fourier analysis was carried out of the unsteady motions for the heave and pitch. For the tanker cases the average accuracy in resistance was 17.5% in the 0^{th} harmonic, while the first harmonic amplitude and phase had errors of 41%D and 6.5%D, respectively. The 0^{th} harmonic of the heave and pitch had an error of 66%, while the first harmonic amplitude and phase differed from the data by 11% and 28% respectively
- For the roll decay the mean error in resistance was around 10%, while the amplitude and period were predicted very well, 0.85% on the average. Waves were predicted rather well by a method using adaptive grids and 4.9M cells, but other methods with coarser grids failed. This complicated case at low Froude number (0.142) calls for larger grids, at least if they are not adapted. This is the case also for the mean velocities in the boundary layer.

7 ACKNOWLEDGEMENTS

The workshop was organized by a committee with six members: the authors and Dr. Emilio Campana, Dr. Suak Ho Van and Prof. Yasuyuki Toda, whose contributions are gratefully acknowledged. Very important contributions have also been made by Lu Zou, who compiled all results and prepared the Proceedings and by Dr. Alessandro Iafrati, who developed and maintained the web site. Prof. Rickard Bensow and Andreas Feymark prepared and compiled the questionnaire and Shanti Bhushan, Hamid Sadat-Hosseini and Maysam Mousaviraad contributed to the specification and analysis of the seakeeping cases. Finally, the great efforts by all workshop participants in the preparation and delivery of all computed results shall not be forgotten.

REFERENCES

[1] L. Larsson, (Ed.) "SSPA-ITTC Workshop on Ship Boundary Layers", SSPA Report 90, Gothenburg, Sweden (1981).

[2] L. Larsson, V.C. Patel, and G. Dyne, (Eds.) "SSPA-CTH-IIHR Workshop on Viscous Flow", Flowtech Research Report 2, Flowtech Int. AB, Gothenburg, Sweden (1991).

[3] Y. Kodama, H. Takeshi, M. Hinatsu, T. Hino, S. Uto, N. Hirata, and S. Murashige, Proceedings, CFD Workshop, Ship Research Institute, Tokyo, Japan (1994).
[4] L. Larsson, F. Stern, and V. Bertram, (Eds.) Gothenburg 2000-A Workshop on Numerical Hydrodynamics, Department of Naval Architecture and Ocean Engineering, Chalmers University of Technology, Gothenburg, Sweden (2002).
[5] L. Larsson, F. Stern and V. Bertram, "Benchmarking of computational fluid dynamics for ship flow: the Gothenburg 2000 Workshop", *J. Ship Research*, Vol. 47: 63-81 (2003)
[6] T. Hino, (Ed.) "2005 Proceedings of CFD Workshop Tokyo 2005", NMRI report (2005).
[7] S.H. Van, W.J. Kim, D.H. Yim, G.T. Kim, C.J. Lee, and J.Y. Eom, "Flow Measurement around a 300K VLCC Model", Proceedings of the Annual Spring Meeting, SNAK, Ulsan, pp. 185-188 (1998a).
[8] S.H. Van, W.J. Kim, G.T. Yim, D.H. Kim, and C.J. Lee, "Experimental Investigation of the Flow Characteristics around Practical Hull Forms", Proceedings 3rd Osaka Colloquium on Advanced CFD Applications to Ship Flow and Hull Form Design, Osaka, Japan (1998b).
[9] W.J., Kim, D.H., Van, and D.H., Kim, "Measurement of Flows around Modern Commercial Ship Models", *Exp. in Fluids*, Vol. 31, pp. 567-578 (2001).
[10] S.J. Lee, H.R. Kim, W.J. Kim, and S.H. Van, "Wind tunnel tests on flow characteristics of the KRISO 3600 TEU Containership and 300K VLCC Double-deck Ship Models", *J. Ship Res*., Vol. 47, No 1, pp. 24-38 (2003).
[11] C. Simonsen, J. Otzen, and F. Stern, "*EFD* and CFD for KCS Heaving and Pitching in Regular Head Waves", Proc. 27th Symp. Naval Hydrodynamics, Seoul, Korea (2008).
[12] A. Olivieri, F. Pistani. A. Avanaini, F. Stern, and R. Penna, "Towing Tank Experiments of Resistance, Sinkage and Trim, Boundary Layer, Wake, and Free Surface Flow around a Naval Combatant INSEAN 2340 Model", Iowa Institute of Hydraulic Research, The University of Iowa, IIHR Report No. 421, pp. 56 (2001).
[13] J. Longo, J. Shao, M. Irvine, and F. Stern, "Phase-Averaged PIV for the Nominal Wake of a Surface Ship in Regular Head Waves", *ASME J. Fluids Eng*, Vol. 129, pp. 524-540 (2007).
[14] M. Irvine, J. Longo, F. Stern, "Towing Tank Tests for Surface Combatant for Free Roll Decay and Coupled Pitch and Heave Motions*",* Proc. 25th ONR Symposium on Naval Hydrodynamics, St Johns, Canada (2004).
[15] F. Stern, K. Agdrup, S.Y. Kim, A.C. Hochbaum, K.P. Rhee, F. Quadvlieg, P. Perdon, T. Hino, R. Broglia, and J. Gorski, "Experience from SIMMAN 2008: The First Workshop on Verification and Validation of Ship Maneuvering Simulation Methods", *Journal of Ship Research*, in press.
[16] L. Larsson, F. Stern, and M. Visonneau, "Gothenburg 2010-A Workshop on Numerical Ship Hydrodynamics", Proceedings Vol. 2, Department of Naval Architecture and Ocean Engineering, Chalmers University of Technology, Gothenburg, Sweden (2010).